The potential of CSP plants for remote communities in the MENA region

Elisa Ghirardi[1*], *Giovanni* Brumana[1] and *Giuseppe* Franchini[1]

[1] University of Bergamo, Department of Engineering and Applied Sciences, 5 Marconi Street, 24044 Dalmine, Italy

Abstract. The present work aims to investigate the load-following capability of a tower-based CSP plant assumed to cover a high fraction (90%) of the power demand of a mid-size remote community. The design of a CRS requires the determination of several variables (number of heliostats, layout arrangement, tower height, receiver dimensions) depending on the solar field size and the site location. In this paper, a two-step optimization procedure is presented. A preliminary optimization is carried out to define the solar field configurations minimizing the budget costs for a range of receiver thermal design powers (from 300 MWth to 1000 MWth). The second optimization, based on annual simulation, selects the storage tank volume, the steam turbine rated power, and the actual reflective area (number of mirrors) capable to cover 90% of the power demand at minimum cost. The analysis is carried out for two load profile and two locations in Egypt. The load profile, compared to the solar radiation availability, determines the relationship between tank capacity and turbine size. The level of radiation has the strongest impact on the oversizing of the solar field and levelized cost of electricity.

1 Introduction

Growing electrical demand is driving the national grid to increasingly severe operating conditions; the existing infrastructures in many regions of MENA are outdated and inadequate transmission capacity leads to frequent blackouts [1]. In addition, there is scarce communication between different networks and ensuring stability becomes critical [2]. The availability of a large amount of renewables could improve the quality of electrification [3] [4], reducing up to 99% of total CO_2 emissions compared to traditional grid and diesel systems [5]. IRENA 2018 report asserts that relying 50% of national generation on concentrating solar power (CSP) plants will increase energy security and improve access to electricity [6]: the embedded storage allows to schedule generation and better accommodate hourly varying demand [7]. Furthermore, the competitiveness of solar technologies is heightened by location with a level of direct normal irradiance (DNI) greater than 3000 kWh/m^2 per year [8].

CSP is also advantaged for applications with isolated networks thanks to the possibility of integration with multi-generation technologies [9]. Ravelli et al. [10] demonstrated the

* Corresponding author: elisa.ghirardi@unibg.it

ability of CSP to meet power and cooling demand in Saudi Arabia; while, Palanzuela et al. emphasized the good integration between CSP and desalination plants, reducing the electricity demand impact of drinking water supply in desert MENA regions [11][12].

The growing interest of the scientific community in central receiver systems (CRSs) over other CSP technologies is justified by higher working temperature level [13], raising plant efficiencies and providing lower storage costs [14]. Despite, higher land occupancy (lower energy density) and financial risk, CRS typically have a more uniform thermal collection capability, all over the year, as reported by Ogunmodimu and Okoroigwe [15].

System performance prediction and hourly behavior must be analyzed in detail to ensure production under different electrical load patterns [16]; Yousefzadeh and Lenzen pointed out the importance of consider partial load operation to avoid system undersized [17]. Wagner et al. showed that a load-following strategy requires thermal energy storage sized according to the operating scheme [18]. Load profile are characterized by different daily and seasonal variation and different ratio of minimum to maximum levels. The electric consumption of a residential complex typically shows large daily and seasonal variations according to people's habits [19], while in an industrial district the demand is approximately constant throughout the year [20]. In the case of large penetration of non-programmable renewables without storage, the back-up generation system (fossil or renewable) must satisfy an energy demand with a typical duck profile characterized by a minimum requirement in central hours and a very steep ramp in the sunset hours [21].

This paper considers a solar power system assumed to serve a remote community and meet almost completely (SF = 90%) the electricity demand. Building on the authors' previous findings on dispatch comparison between CSP systems [22] and detailed design of CRS systems [23,24], several operating conditions are considered to assess the production flexibility of the solutions.

2 Model description

The models developed for the CSP system simulation and the performance of the solar technologies are based on Trnsys v.18 and plant operation are simulated over one-year period.

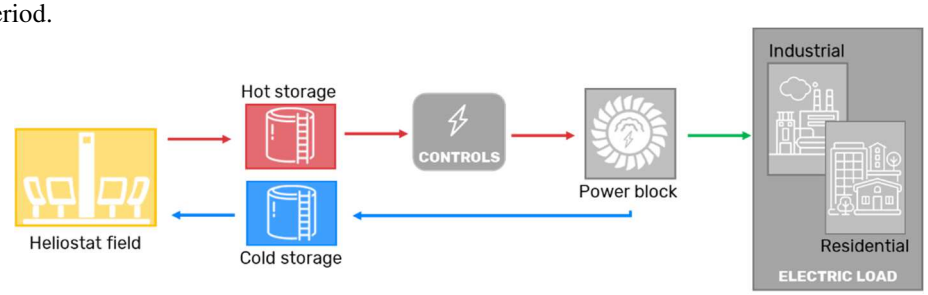

Fig. 1. Schematization of CSP plant structure.

A schematic of the structure of the CSP system is shown in Fig. 1. The model includes the solar field and a two-tank direct thermal energy storage; a mixture of molten salts (60% $NaNO_3$ - 40% KNO_3) is considered as the heat transfer fluid. According to the available radiation, a mass flow is sent from the cold tank to the solar field to provide a temperature rise from 300°C to 550°C. The hot tank stores the excess of molten salt production and, using a management system, delivers enough flow to the steam generator to meet the hourly demand. The actual discharge rate of the TES is affected by the efficiency of the associated Rankine cycle: in the present work, the performance of the steam turbine is evaluated according to the approximations reported by Poullikkas et al. [25], without providing any details of the operating parameters. The power block design efficiency is determined

according to a rated power while its variation is evaluated including the effect of ambient temperature and at part load. The interpolation function adopted (dashed line in Fig. 2a), fits the curve proposed by Poullikkas (solid line) in the range 500 kWe - 100 MWe, with a coefficient of determination of 0.99. Fig. 2b shows the operating map, including derating at partial load and ambient temperature for condenser performance, normalized to a reference condition of 100% load and 30°C. Starting from a selected rated power, the software combines the two maps and evaluates the performance based on the operating conditions.

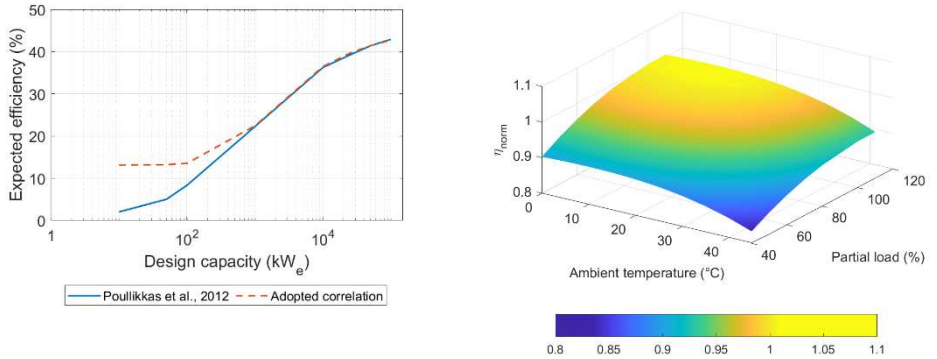

(a) Variation with turbine size (b) Variation with operative condition

Fig. 2. Thermal efficiency map of the power block.

2.1.1 Solar field

A radial staggered surrounding heliostat field reflects the radiation to an external cylindrical receiver. The optical efficiency of each heliostat η_{helio} is evaluated according to the Eq. 1, and the field efficiency η_{field} is the average of the efficiencies of the mirrors in the final layout. The detail of each losses calculation has given in [24].

$$\eta_{helio}\,(x,y,t) = \rho(t) \cdot f_{cos}\;(x,y,t) \cdot f_{att}\,(x,y,t) \cdot f_{spill}\,(x,y,t) \cdot f_{sb}\,(x,y,t) \quad (1)$$

In order to determine the optimal configuration for the entire solar production system, it is necessary to explore different values of reflective area aperture, a parameter closely related to the design thermal power of the field. The CRS performance is not linearly scalable for different power output since the contribute of each component is variable with the design power (such as the number of heliostats ($Nhelio$), the layout arrangement, the tower height (Ht) and the receiver dimensions (D_{rec}, HD_{rec})) [23]. For this reason, a preliminary optimization has been carried out determining the heliostat field-receiver structure that minimize the cost for a wide range of design thermal power delivered to the HTF (from 300 MWth to 1000 MWth).

2.1.2 Solar field optimization procedure

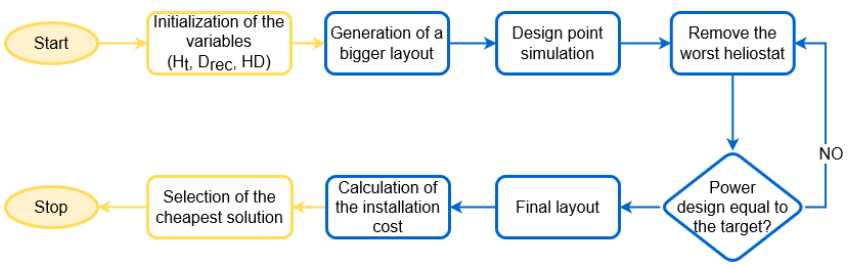

Fig. 2. Schematization of the optimization procedure.

The economic optimization procedure (schematized in Fig. 2), repeated for all the power considered, is detailed below. It is worth noting that, having imposed the output power, the combination that minimizes CapEx or LCOE are equivalent.

1. For the selected set of variables (namely H_t, D_{rec}, HD_{rec}), a bigger heliostat field is generated. The adopted geometric parameters (i.e. the radial increments shown in Fig. 3) were previously optimized for different numbers of heliostats in the field in order to maximize field efficiency, as presented in [23,24].

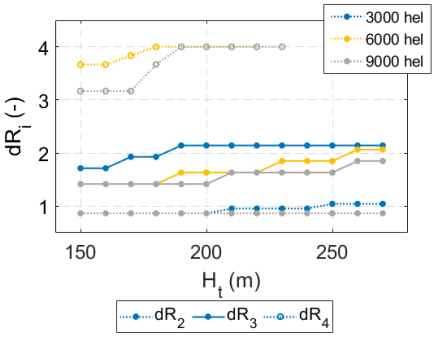

Fig. 3. Radial increments for different heliostat field size.

2. The generated layout has been simulated under design point condition in order to evaluate single mirror efficiency (Eq. 1), the receiver thermal efficiency (Eq. 2), and the total absorption efficiency (Eq. 3) that combines the performance of the solar field and the receiver.

$$\eta_{rec}\,(t) = \alpha_{rec} - (\varepsilon\sigma A_{rec}(T_{wall}^4 - T_{amb}^4) + h_{mix}A_{rec}(T_{wall} - T_{amb}))/E_{inc} \quad (2)$$

$$\eta_{abs}\,(t) = \eta_{field}(t) \cdot \eta_{rec}(t) \quad (3)$$

3. The worst heliostats are deleted until the power delivered to the receiver is equal to the target power.
4. For each combination the installation cost is calculated according to eq. 4.

$$Plant_{cost} = C_{helio} + C_{tower} + C_{rec} + C_{PB} + Land_{cost} \quad (4)$$

Table 1. Specification of the financial and economic values.

Component	Cost model	
Heliostat	$156 \cdot Nhel \cdot Area_{hel}$	$\$/m^2$
Tower	$3E6\ exp\ (0.0113(Ht - H_{rec}/2))$	$\$/m$
Receiver	$1.03E8\ (Area_{rec}/1571\ )^{0.7}$	$\$/m^2$
Power block	$1.33 \cdot P_{nom}$	$\$/MWe$
Land	$1.25 \cdot Area_{land}$	$\$/m^2$

5. The solution that minimizes the cost for each power considered is selected. Although the flux at the receiver surface is not analyzed in detail, a constant pointing strategy - equal to 2 - is adopted to guarantees a more uniform distribution for most of the operating period [26]; receiver sizes that do not ensure the 1.1 MW/m^2 flux limit are discarded.

The analyzed variables and their range of variation is reported in table 2.

Table 2. Definition of the search space.

Variable	Unit	Range	Step
Ht	m	150-270	10
D_{rec}	m	11-20	0.5
HD_{rec}	-	1-1.2	0.1

2.1.3 Solar field optimization results

The main resulting geometric parameters are summarized in Fig. 4 along with the trend in efficiency and total installation cost. The number of heliostats selected is directly proportional to the required power (Fig. 4a), as is the receiver absorption area (Fig. 4b); whereas the optimal tower height remains constant for 100 - 150 MWth intervals as reported in Fig. 4c. The behavior of the occupied land (Fig. 4d) is consistent with changes in tower height, which confirms the strong influence of Ht on the layout. The trend in efficiency, shown in Fig. 4e, is mostly in agreement with the change in tower height (the largest discontinuities are shown for 500 MWth and 850 MWth), while for powers above 900 MWth a slight influence of the receiver area is observed. Regarding the total cost of the systems, an almost linear trend is observed with power, while the cost per unit of reflecting area is slightly lower when the power considered is higher: the cost of the tower and receiver are of less impact when the number of heliostats in the field is higher.

Although many codes and algorithms are dedicated to the detailed calculation of optical losses, including cosine effect, blocking and shadowing, mirror reflectivity, spillage, and atmospheric attenuation [27,28], the main parameters affecting the hourly efficiency of the field are the size of the system, i.e. the mirror aperture area and tower height, and the zenith angle. The performance of the heliostat subsystem has been simplified with an efficiency map, which is provided to the CSP model adopted in the paper, reducing the computational cost but providing good accuracy. For each design power, the field efficiency was calculated according to Eq. 1; the resulting map is shown graphically in Fig. 5. For the sake of completeness, the maximum efficiency reached in different month is highlighted in Fig. 6: a general flat trend is observed from March to September with a limited reduction (<0.4%) in the central months (this behavior, resulting from the optimization assumptions, has already been commented in the paper [24]). The main irregularities with the size correspond to the trend shown in Fig. 4e.

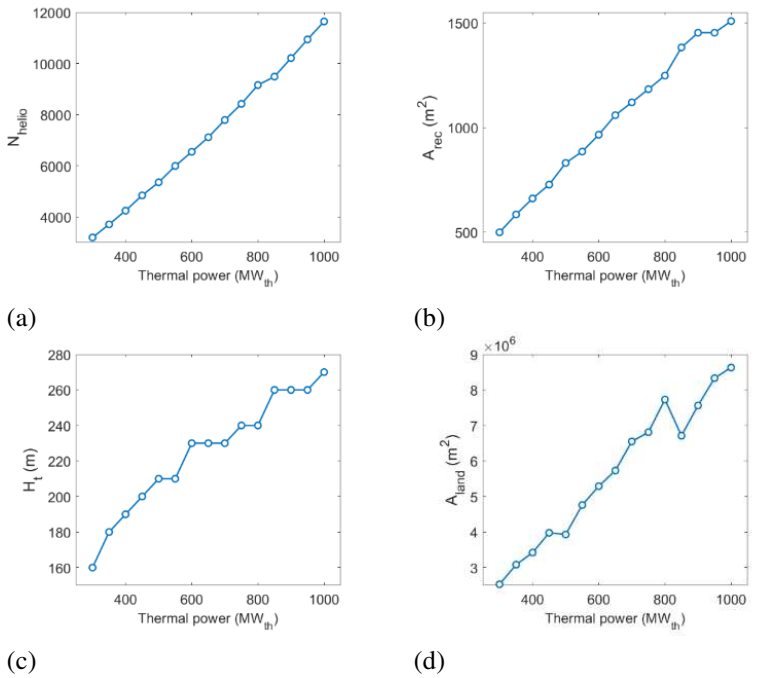

Continued on next page

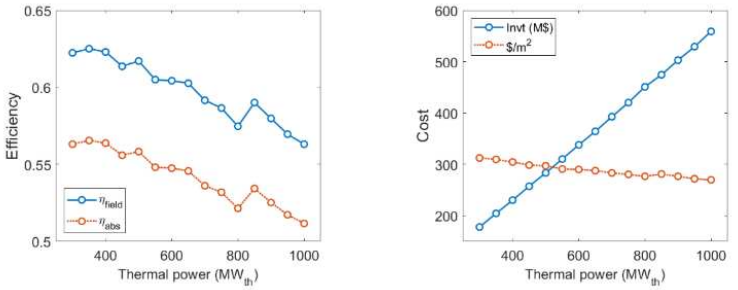

(e) (f)

Fig. 4. Optimal parameters of different design thermal power.

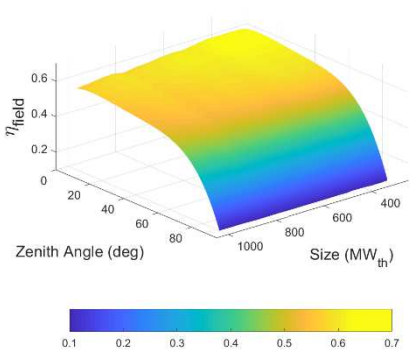

Fig. 5. Heliostat efficiency map with size and Solar Zenith angle.

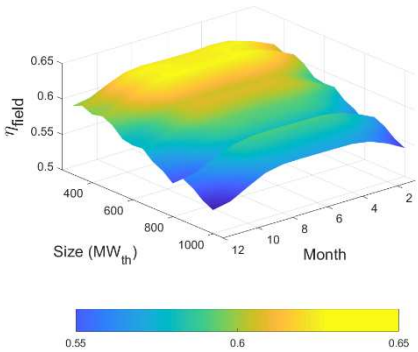

Fig. 6. Monthly variation of the peak efficiency for different size.

3 Production system optimization procedure

The results obtained in the previous paragraph in terms of the solar field are now applied to the optimization of the system: based on the size of the heliostat field, all other variables of the solar array are considered fixed. The solar field aperture area $A_{solarfield}$, the storage capacity h_{tank} and the turbine nominal power P_{PB} have been determined through an optimization procedure to minimize the budget cost function and ensuring a portion of energy demand of 90% supplied by the solar technology (Solar Fraction - SF). The size of the solar field and design output of the turbine are chosen independently in order to enable the optimizer to determine the best combination between Solar Multiple and storage capacity. The optimization algorithm (direct search pattern method) is implemented with the tool GenOpt that runs multiple Trnsys simulations changing the search pattern of the variables. The combination of reflective area, hours of full tank and turbine nominal power that are analyzed in the optimization procedure are included in the search space reported in Tab. 3.

The considered unit costs shown in Tab. 3 have been estimated according to the economic data reported by the NREL in the System Advisor Model [29]. The objective function, corresponded to the direct capital cost of the plant (C), is calculated according to Eq. 5 and includes: the solar field (derived from the previous optimization shown above), the tank system C_{tank} and the power block C_{PB}. The tank capacity is calculated as the maximum available hours of turbine operation h_{tank} at its nominal capacity P_{PB}. The software SAM listed the molten salt TES and the steam turbine costs equal to 22 $/kWh and 1440 $/kW, respectively. The proposed model includes a variable budged cost according to the nominal capacity of the power block ($/kW), as presented by Poullikkas and al. [25]. The reported

power block cost correlation has been modified in order to align the installed cost with the value reported by SAM at the same nominal capacity of 100 MW. The parameter p is a penalty cost related to the energy deficit (seen as $SF - SF_{target}$), that gives different "cost" to energy deficit or surplus (Eq. 6); this function structure allows to reject all system configurations that cannot satisfy the power request and avoid an excessive oversizing of the system. Finally, to correctly compare the economic performance of different technologies the LCOE function is considered (Eq. 7). The adopted financial parameters are resumed in table 4.

Table 3. Budget cost and search space of CSP component.

Component	Cost model		Search space	
			Start value – min – max – step	
Solar field	$324 - 2.74 \cdot 10^{-5} \cdot A_{refl}$	$\$/m^2$	0.86 – 0.5 – 4.2 – 0.1	km^2
Tank	22	$\$/kWh$	12 – 6 – 24 – 1	h
Power block	$15587 \cdot P_{PB}^{-0.232}$	$\$/MW_e$	75 – 20 – 150 – 2.5	MW_e

$$C = C_{solar\ field} + h_{tank} \cdot P_{PB} \cdot C_{tank} + C_{PB} + p \tag{5}$$

$$p = \begin{cases} 3.6 - 4 \cdot SF & SF \leq 90\% \\ 1.5 \cdot SF - 1.35 & SF > 90\% \end{cases} \tag{6}$$

$$LCOE = \frac{\frac{i(1+i)^{Ny}}{(1+i)^{Ny-1}} C + OM_{fixed}}{E_{el}} + OM_{var} \tag{7}$$

Table 4. Financial parameters.

Parameters	Value	Unit
Lifetime Ny	30	year
Interest rate i	4	-
OM_{fixed}	66	$\$/kW\ -yr$
OM_{var}	3.5	$\$/MWh$

4 Case study

This work investigates the load-following capability of different CRS plant to satisfy the load demand of a mid-size town located in Egypt. Environmental conditions in Egypt allow solar technologies to be more competitive: direct normal irradiance (DNI) reaches levels between 2000-3200 kWh/m^2 per year and an average of 9-11 hours of solar activity [1]. Two locations are compared: Aswan and Giza, with quite different weather conditions, as shown in Fig.7, for two representative days of summer and winter. Figure 7a shows the average monthly temperature and relative humidity. Aswan shows a large range between maximum and minimum temperature, while humidity is very low in both the summer and winter periods. This results is a reduced diffusion of available solar radiation and, as a result, concentrating solar devices operate with better efficiency. Giza, on the contrary, has a reduced peak temperature in summer, which benefits the efficiency of the steam turbine, but a much higher humidity level (about 60%) which penalizes the available radiation. From the Meteonorm database [30], the annual amount of DNI is 3058 kWh/m^2 and 2097 kWh/m^2 for Aswan and Giza, respectively. In addition, the proposed locations show contrasting seasonal patterns of DNI, as presented in Fig. 7b. Giza shows a typical bell-shaped distribution with a peak of radiation in summer and a high decrease (50%) during the winter period. In contrast, Aswan's radiation has a more constant pattern, peaking in winter (250 kWh/m^2).

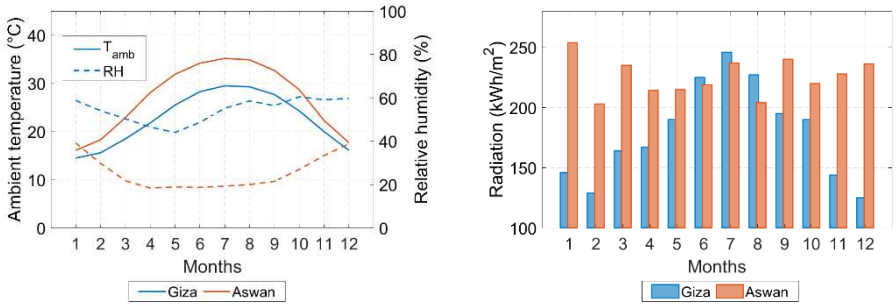

(a) Ambient temperature and relative humidity (b) DNI

Fig. 7. Ambient condition comparison for the investigated location, Giza and Aswan.

Furthermore, according to different establishment, two different electric load profile are adopted in the model with consistent power demand fluctuation in in terms of daily and monthly variations. Fig.8 shows the trend for two typical days, one summer and one winter, of two electrical loads with different characteristics. In detail, in the presence of a predominantly residential user, the load curve is strongly influenced by the use of air conditioning equipment - in phase with the variation of ambient temperature: there is a moderate reduction of 40% between the peak value between summer and winter and at the same time a large variation in demand over the day (the minimum is about 30-50% lower than the peak). In industrial complexes, on the contrary, the maximum level is reached in the winter season and, even during the night, the demand is quite high (only 30% smaller than the daily peak); moreover, the seasonal variation is limited to 15%. The load models proposed here were presented in [31] and were scaled to achieve the same 100 MW peak load, resulting in a different annual integral value (540 GWh vs. 700 GWh).

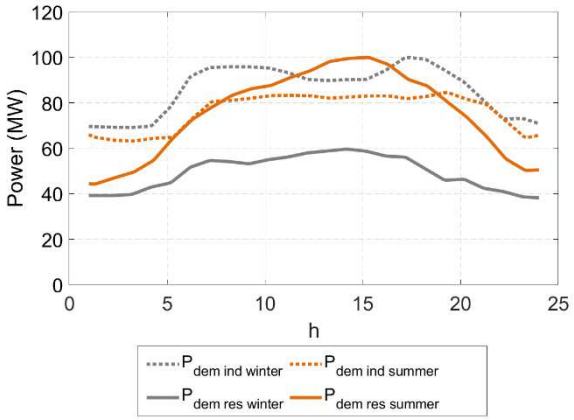

Fig. 8. Industrial and residential load profile for summer and winter days.

5 Results and discussion

The results of the optimization procedure are summarized in Table 5, the load following capability is studied for two load profile models (i.e., residential and industrial) together with the influence of climatic conditions (the analysis is repeated for Giza and Aswan).

The environmental conditions in Giza severely penalize the solar field performance, which requires a 55-62% larger reflective area to meet the 90% demand level. In addition, 60% greater storage capacity is required for both load profiles. The Aswan condition allows

the solar field and storage not to be oversized and a solar multiple of 2.4 is obtained (close to the best practice suggestion); in contrast, for Giza the SM is much larger, about 4 (60% larger). The solar aperture area and the capacity of the TES system are, in general, larger in the industrial case (20%-28% and 30%-28%, respectively for Giza and Aswan) due to the need to meet higher demand even during the night and winter period; the power block size also seems to be site independent: the 20-22% larger steam turbine capacity indicates that the industrial load forces to provide a higher level of power to guarantee the annual energy demand.

In terms of overall cost, the residential case is 18-24% cheaper than the industrial case, and Aswan, due to the higher radiation available, appears to be cheaper (-35%). More in detail, for Giza, the solar array is responsible for more than 60-65% of the overall cost; in Aswan weather conditions, the impact of the solar field is reduced to 50-55% and the power block effect becomes more notable (up to 17%).

Table 5. Optimized component size for each combination.

Objective function		Giza		Aswan	
		Res	Ind	Res	Ind
A_{refl}	m^2	1386442	1947320	861876	1066754
Cap_{tank}	MWh	1141	1564	683	968
h_{tank}*	h	7.5	8.1	4.4	5.1
PB_{size}	MW_e	63.5	82	65	80
SM	-	3.9	4.05	2.4	2.6
$Capital\ cost$	$M	650.5	860.8	441.1	539.1
* Tank capacity expressed in equivalent hours of steam turbine operation at rated load					

5.1 Daily simulation

The simulation results of the analyzed combinations are now compared to investigate which load tracking strategy was preferred based on the considered case. Figure 9 shows hourly results for each plant configuration and load pattern. The graphs show the heat collected (Q_{coll}), instantaneous demand ($Load$), and actual power delivered (CRS_{prod}), for two representative summer (left graphs) and winter (right graphs) days. In addition, the level of the hot tank is also reported.

The Giza radiation condition leads to a significant difference in performance in the two seasons: for many hours per day during the summer months, a fraction of the heliostat field must be defocused, since the heat storage tank has reached its maximum capacity. On the contrary, in the winter period, the radiation level is not sufficient to exploit the full capacity of the tank and on some days it is not possible to charge it more than 50%. Fig. 9a shows that in the residential case, although the accumulation level is always above 40%, the limited size of the power block does not allow to guarantee the maximum demand. The industrial load emphasizes the oversizing of the field: as depicted in Fig. 9b the production reaches almost 790 MW while the thermal demand of the power block is only 230 MW (equivalent to 90 MW_e); this behavior is justified by the need to fully satisfy the demand in summer to compensate for the low radiation in winter when the demand is higher.

The Aswan condition ensures a more uniform performance of the CRS system throughout the year. Good radiation in winter allows for a smaller turbine: the entire load does not need to be met in summer to achieve the required SF. Moreover, the smaller tank is better exploited by performing complete charge and discharge cycles. In the residential load case (Fig. 9c), solar irradiation and power demand profiles appear to be in phase and there is no need to

oversize the turbine, similarly to Giza. Moving to the industrial case (Fig. 9d), the chart highlights that, for a few hours, the hot reservoir is empty and the peak demand in the early morning may not be met.

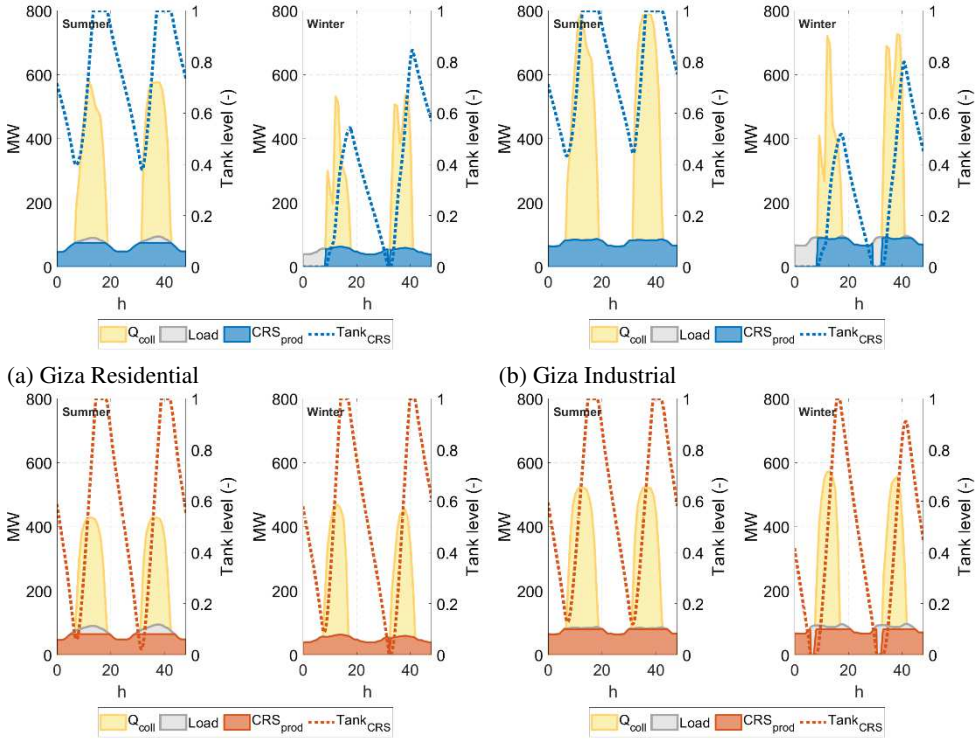

(a) Giza Residential (b) Giza Industrial

(c) Aswan Residential (d) Aswan Industrial

Fig. 9. Daily simulation results.

5.2 Annual performance

Figure 10 shows the monthly energy quantities, i.e. the electricity produced by the plant in the two locations ("Giza" and "Asw") and the load demand (Load), for the two electric profiles. In general, depending on the solutions, a different management of the allowed energy deficit (10% of the demand) is observed. Under the Aswan condition, the performances are more uniform throughout the year and the biggest differences with respect to Giza are reported for the residential case (Fig. 10a): in fact, for Aswan the maximum deficit of 15% occurs in the central months while from November to April more than 90% of the monthly demand is satisfied (up to 96% in February); on the contrary, for Giza almost 95% of the production is ensured in summer months to compensate the worst conditions in winter, where up to 29% deficit is achieved. Industrial loading (Fig. 10b) minimizes the deficit in the summer months, and oversizing the solar field, for Giza conditions, allows to supply the full demand from May to October; however, the deficit is more than 10-20% from November to February, reaching a maximum level in December of 36% and 22% for Giza and Aswan, respectively.

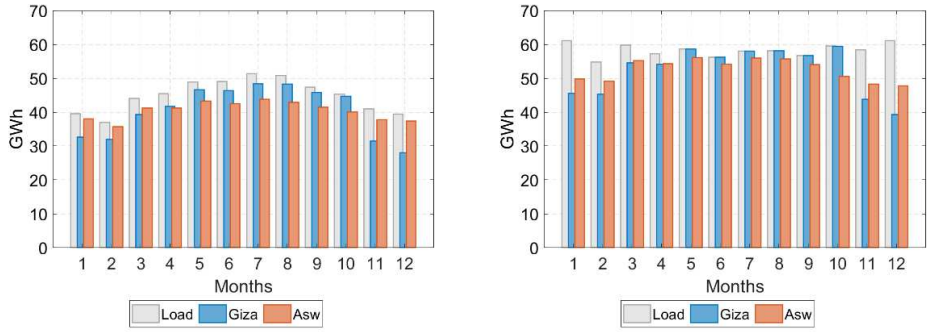

(a) Residential (b) Industrial

Fig. 10. Monthly simulation results.

In order to comprehensively evaluate the performance of the studied configurations, the annual energy balance is shown in Table 6. Looking at the energy losses due to defocus, defined as the percentage of the collected energy, a maximum surplus of 16% is observed for the industrial case in Giza that slightly decreases to 6.3% switching to residential load; in the Aswan condition, the heat surplus is limited to almost 1.5% for both loads. In addition, the different condition between the two cities has a minor impact on turbine efficiency; the higher temperature in Aswan only increases heat demand by 1%.

Finally, the economic feasibility of the solutions is considered. According to the results in Tab. 5, the generation solution for the residential case in Aswan has the lowest CapEx; the introduction of the LCOE function corrects the comparison between the scenarios and the higher energy demand of the industrial cases allows a larger amortization of the initial investment: from a 20% higher cost, a 5% saving in terms of LCOE is obtained. The influence of irradiation on the cost of electricity is underlined by the difference of more than 30% between the facilities in the two cities.

Table 6. Financial parameters

		Giza		Aswan	
		Res	Ind	Res	Ind
Solar energy	*GWh*	2908.3	4084.9	2636.3	4084.9
Collected energy	*GWh*	1299.9	1774.9	1286.7	1576.6
Heat demand	*GWh*	1300.0	1655.8	1312.2	1672.7
Energy surplus	%	6.3	16	1.4	1.6
LCOE	$/kWh$	0.0992	0.0988	0.0696	0.0657

6 Conclusion

The production flexibility of CRS plants has been evaluated under different operating conditions in order to analyze the feasibility of the proposed system in remote areas. The investigation has been carried out for two different power demand patterns, correspondent to industrial or residential settlements, and for two cities (Giza and Aswan) with different available radiation and ambient conditions. The solution that guarantee 90% of the electric demand has been optimized in terms of solar field area, tank capacity and power block size in order to provide the minimum investment cost. The dimensions of all the component, responsible for conversion from radiation to thermal energy, has been determined with a preliminary optimization as function of the reflecting area only, minimizing the cost.

It has been found that the lower irradiation available in Giza leads to an oversized solar array with a solar multiple of almost 4, while in Aswan climatic conditions the SM is reduced to about 2.5. The residential load has a daily profile similar to the solar radiation, with a

maximum around noon: this allows for reduced reservoir and turbine size. In contrast, energy demand is more constant in the industrial load model, with high demand at night, thus requiring 30% more storage capacity. The higher level of irradiation of Aswan, especially in winter compared to Giza, allows a better management of the supply/demand ratio during the year and also to minimize losses due to field defocusing; at the same time it allows to reduce the cost of electricity, reaching a minimum of 6.6 c$/kWh.

References

1. RES4MED, (2015)
2. K. E. Okedu and W. Z. A. L. Salmani, **3**, (2019)
3. Y. M. Seshie, K. E. N'Tsoukpoe, P. Neveu, Y. Coulibaly, and Y. K. Azoumah, Renew. Sustain. Energy Rev. **90**, 195 (2018)
4. G. Prinsloo, R. Dobson, and A. Mammoli, Curr. Altern. Energy **2**, 2 (2018)
5. S. Goel and R. Sharma, Renew. Sustain. Energy Rev. **78**, 1378 (2017)
6. IRENA, *Renewable Energy Outlook: Egypt* (2018)
7. G. Iaquaniello, W. Montanari, and A. Salladini, Sol. Energy **157**, 1056 (2017)
8. W. E. Alnaser and N. W. Alnaser, in *Innov. Renew. Energy* (2020), pp. 167–183
9. R. Leiva-Illanes, R. Escobar, J. M. Cardemil, D. C. Alarcón-Padilla, J. Uche, and A. Martínez, Energy Convers. Manag. **179**, 249 (2019)
10. S. Ravelli, G. Franchini, and A. Perdichizzi, Renew. Energy **121**, 712 (2018)
11. N. Ghaffour, S. Lattemann, T. Missimer, K. C. Ng, S. Sinha, and G. Amy, Appl. Energy (2014)
12. P. Palenzuela and D. C. Alarcón-Padilla, in (2019), pp. 327–340
13. C. K. Ho, Sol. Energy **152**, 38 (2017)
14. K. R. Bhargav, F. Gross, and P. Schramek, Energy Procedia **49**, 40 (2013)
15. O. Ogunmodimu and E. C. Okoroigwe, Renew. Sustain. Energy Rev. **90**, 104 (2018)
16. M. Shepero, D. van der Meer, J. Munkhammar, and J. Widén, Appl. Energy **218**, 159 (2018)
17. M. Yousefzadeh and M. Lenzen, Renew. Sustain. Energy Rev. **114**, 109342 (2019)
18. M. J. Wagner, A. M. Newman, W. T. Hamilton, and R. J. Braun, Appl. Energy **203**, 959 (2017)
19. A. Grandjean, J. Adnot, and G. Binet, Renew. Sustain. Energy Rev. **16**, 6539 (2012)
20. A. Vaghefi, F. Farzan, and M. A. Jafari, Appl. Energy **158**, 378 (2015)
21. H. Price, D. Kearney, F. Redell, R. Charles, and F. Morse, in (2018), p. 040032
22. G. Brumana, G. Franchini, and E. Ghirardi, Energy Procedia **148**, 615 (2018)
23. E. Ghirardi, G. Brumana, and G. Franchini, E3S Web Conf. **197**, 08017 (2020)
24. E. Ghirardi, G. Brumana, G. Franchini, and A. Perdichizzi, Renew. Energy **168**, 393 (2021)
25. A. Poullikkas, C. Rouvas, I. Hadjipaschalis, and G. Kourtis, Int. J. Energy Environ. **3**, 9 (2012)
26. J. Servert, A. González, J. Gil, D. López, J. F. Funes, and A. Jurado, in *AIP Conf. Proc.* (2017), p. 030047
27. N. C. Cruz, J. L. Redondo, M. Berenguel, J. D. Álvarez, and P. M. Ortigosa, Renew. Sustain. Energy Rev. **72**, 1001 (2017)
28. J. García-Barberena, A. Mutuberria, L. G. Palacin, J. L. Sanz, D. Pereira, A. Bernardos, M. Sanchez, and A. R. Rocha, AIP Conf. Proc. **1850**, (2017)
29. M. J. Wagner, Simulation and Predictive Performance Modeling of Utility-Scale Central Receiver System Power Plants, 2008

30. J. Remund, S. Müller, S. Kunz, B. Huguenin-Landl, C. Studer, D. Klauser, C. Schilter, and R. Lehnherr, *Meteonorm Handbook* (2012)
31. G. Franchini, A. Perdichizzi, and S. Ravelli, in *Power-Gen Africa 2016* (Johannesburg, South Africa, 2016), pp. 1–12